Proceedings of ASME Turbo Expo 2011
GT2011
June 6-10, 2011, Vancouver, British Columbia, Canada

GT2011-46722

TWO- AND THREE-DIMENSIONAL PRESCRIBED SURFACE CURVATURE DISTRIBUTION BLADE DESIGN (CIRCLE) METHOD FOR THE DESIGN OF HIGH EFFICIENCY TURBINES, COMPRESSORS, AND ISOLATED AIRFOILS

T. Korakianitis*, **I. A. Hamakhan**, **M. A. Rezaienia**, **A. P. S. Wheeler**
School of Engineering and Materials Science
Queen Mary, University of London
London, E1 4NS, UK

ABSTRACT

The prescribed surface curvature distribution blade design (CIRCLE) method is presented for the design of two-dimensional (2D) and three-dimensional (3D) blades for axial compressors and turbines, and isolated blades or airfoils. The original axial turbine blade design method is improved, allowing it to use any leading-edge (LE) and trailing-edge (TE) shapes, such as circles and ellipses. The method to connect these LE and TE shapes to the remaining blade surfaces with curvature and slope of curvature continuity everywhere along the streamwise blade length, while concurrently overcoming the "wiggle" problems of higher-order polynomials is presented. This allows smooth surface pressure distributions, and easy integration of the CIRCLE method in heuristic blade-optimization methods. The method is further extended to 2D and 3D compressor blades and isolated airfoil geometries providing smooth variation of key blade parameters such as inlet and outlet flow angles, stagger angle, throat diameter, LE and TE radii etc. from hub to tip. One sample 3D turbine blade geometry is presented. The efficacy of the method is examined by redesigning select blade geometries and numerically evaluating pressure-loss reduction at design and off-design conditions from the original blades: two typical 2D turbine blades; two typical 2D compressor blades; and one typical 2D isolated airfoil blade geometries are redesigned and evaluated with this method. Further extension of the method for centrifugal or mixed-flow impeller geometries is a coordinate transformation. It is concluded that the CIRCLE method is a robust tool for the design of high-efficiency turbomachinery blades.

NOMENCLATURE

b axial chord (nondimensionally b=1)
c blade chord, leading to trailing edge
$c_0, c_1 \ldots$ thickness coefficients (eqns. 6,9)
$C1, C2 \ldots$ Bezier control points (fig. 1d)
$\mathbf{C} = 1/r$ curvature (eqn. 1 and fig. 1d)
C_D drag coefficient (eqn. 4)
C_L tangential-loading (lift) coefficient (eqn. 5)
C_p pressure coefficient (eqn. 10)
i incidence
$k_1, k_2 \ldots$ exponential thickness polynomials (eqns. 6,9)
M Mach number
o throat circle (fig. 1a)
p pressure
P points or nodes on the blade surfaces
r local radius of curvature (eqn. 1)
Rey Reynolds number
S tangential pitch of the 2D blades (fig. 1)
(x,y) Cartesian coordinates
(X,Y) nondimensionalized coordinates (with b)
$y1,\ y2\ y3$ blade segments: leading edge; main CIRCLE part; and trailing edge (figs 1, 2 and 3)
$Y_L \equiv (p_{o,in} - p_{o,ot})/(p_{o,in} - p_{st,ot})$, pressure loss coefficient
z length along 3D blade height
z' (length along 3D blade height) / (blade height)
$Z_L \equiv (p_{o,in} - p_{o,ot})/p_{o,in}$, stagnation pressure loss factor

*Corresponding author. Email forward for life: *korakianitis@alum.mit.edu*

Greek

α flow angle
β blade-surface angle
λ stagger angle of the blades
ϕ angle of throat diameter (figs. 1 and 2)
$\xi 1, \psi 1$ to $\xi 5, \psi 5$ variables specifying the 3D-distribution of 2D-section parameters (fig. 1d)

Subscripts

cmb camber line
crd chord line
in blade inlet region
is isentropic (M_{is} in fig. 6)
o stagnation
ot blade outlet region
p pressure side
*p*2 pressure side TE circle to *y*1 segment (figs 1, 2 and 3)
pm pressure side *y*1 to *y*2 segments (figs 1, 2 and 3)
pk pressure side *y*2 to *y*3 segments (figs 1, 2 and 3)
*p*1 pressure side *y*3 segment to LE circle (figs 1, 2 and 3)
s suction side
*s*2 suction side TE circle to *y*1 segment (figs 1, 2 and 3)
sm suction side *y*1 to *y*2 segments (figs 1, 2 and 3)
sk suction side *y*2 to *y*3 segments (figs 1, 2 and 3)
*s*1 suction side *y*3 segment to LE circle (figs 1, 2 and 3)
st static

INTRODUCTION

The design of turbomachines is constrained by considerations of limited Mach numbers, minimizing the number of stages, while maintaining structural integrity, high efficiencies, and meeting other thermoeconomic constraints, e.g. [1]. Initial engine-component designs are based on assumptions of steady quasi 3D axisymmetric flow via throughflow analyses (e.g. [2,3]) in a series of meridional planes, concluding with 3D velocity diagrams for each blade row from hub to tip. The blade shapes are then designed by "stacking" 2D blade designs using rules for the locus of the centers of gravity of the 2D sections and the 3D shape of the leading edge, the trailing edge, and resulting blade surfaces, or lately by 3D computational fluid dynamics (CFD) solutions and selective local "zooming" [4]. Compromises in performance must be made to accommodate these three-dimensional constraints, material strength considerations, the location of cooling passages and hollow sections, etc.

Various investigators use different definitions for blade design methods: direct; inverse, semi-inverse, full-inverse or full-optimization methods [5]; analysis and design modes [6]; optimization and design methods [7].

We define as direct the method in which the designer inputs the geometry of the blade and the output is the performance (from an analysis code) in terms of surface pressure distributions or isentropic surface Mach-number distributions. The performance provides guidelines for where to increase or decrease the loading, and how to modify the surface geometry in successive iterations, until a desirable performance is obtained from the analysis code. We also define as inverse the various methods in which the designer specifies the performance of the blade to obtain the geometry, or modifications to a portion of the surface velocity or pressure distribution to obtain modifications to the geometry. This latter definition includes what other investigators define as fully-inverse, semi-inverse, adjoint, or simply design methods.

Both methods have relative advantages and disadvantages. In the direct method, it is relatively easy to fulfill mechanical and geometric constraints; but it is usually laborious to obtain the desired distribution of pressure or velocity along the blade profile. On the other hand, it can be difficult to obtain an acceptable geometry with an inverse method [8–11]. The non-heuristic inverse design method (mathematical inversion of pressure distribution to surface geometry) has difficulties in both of the leading and trailing edges, due to the mathematical singularity (zero velocity) at the two stagnation points [11,12] and results in blades with zero thickness at the trailing edge, which are impossible to manufacture; or with other adaptations made at the trailing edge introducing uncertainties. This last difficulty makes the non-heuristic inverse method acceptable for some compressor blade geometries of thin trailing edge, but unacceptable for turbine geometries that have thicker trailing edges. Both the direct and inverse methods, including the CIRCLE method, can be coupled with various hybrid multi-objective heuristic or evolutionary-algorithm optimization techniques in order to optimize various aspects of compressor, turbine and hydraulic pump blade shapes and airfoils, e.g. [13–18].

This paper introduces a method to take the design from initial throughflow calculations to specifying the 2D and 3D blade shapes with continuity in surface curvature and slope of surface curvature from LE to TE, and therefore enables design for inherently good aerodynamic performance. The method can be used to provide finished blade designs of high efficiency, as illustrated in later examples. Alternatively, it can also be used to provide initial geometries for other direct and inverse design methods, or to provide geometries for optimization methods with genetic and heuristic algorithms. The CIRCLE method is based on modifications to the earlier 2D blade-design method [19–23] and its earlier 3D extensions [24] that allow the designer to include 3D LE and TE circles or ellipses, while maintaining continuous slope of curvature everywhere (2D and 3D) on the blade surfaces. The CIRCLE method starts from the TE shape and designs the 2D blade shape in three line segments: *y*1 near the LE; *y*2 in the middle part of the surface; and *y*3 near the TE. By specification the method ensures blade-surface curvature and slope-of-curvature continuity from the LE stagnation point to the TE stagnation point. Application of the method to remove LE spikes and smooth LE flow "disturbances" from 2D turbine blades has been published in [25]. In this paper the CIRCLE method is applied to the design of 2D and 3D turbine and compressor blades, and 2D airfoils. The streamwise blade-surface curvature distribution is manipulated to optimize the aerodynamic performance of 2D sections. 2D shapes are designed near hub, mean and tip regions, and the 3D blade shape is designed by smoothly (again with curvature continuity) varying the 2D parameters from hub to tip.

This is a new design environment decoupling the traditional maximum thickness and maximum camber discussions (used in early airfoil designs) from blade design. Similarly to inverse design methods, the CIRCLE method is guided by the surface pressure and surface Mach number distributions with their relation to surface-curvature distribution, and the output is the blade shape. The design sequence shapes the surface curvature and with it the location of maximum loading, forwards or backwards, on the blade surface. The advantages of the CIRCLE blade design method are illustrated with several examples in axial turbines, axial compressors and one isolated airfoil.

IMPORTANCE OF STREAMWISE BLADE SURFACE CURVATURE

The theoretical and experimental evidence that both curvature and slope of curvature affect boundary-layer development and aerodynamic performance has been presented in [21–23], and is further justified in the blade re-designs in the following. The boundary layer does not shield the core of the flow from surface curvature discontinuities because there is a strong dependence of local boundary layer pressure and velocity on local radius of curvature. Smooth streamwise blade-surface pressure distributions (avoiding local accelerations and decelerations) require smooth surface-curvature distributions (continuous slopes of pressure and curvature along the blade surface). Continuous slope of curvature requires continuous third derivatives at the splines or surface patches used to design the blades as illustrated in the following two equations for curvature $\mathbf{C}$ and slope of curvature $\mathbf{C}'$ for blade-surface line segments $y = f(x)$, $y' = df(x)/dx$, $y'' = d^2f(x)/dx^2$ and $y''' = d^3f(x)/dx^3$.

$$\mathbf{C} = \frac{1}{r} = \frac{y''}{\left[1+y'^2\right]^{(3/2)}} \tag{1}$$

$$\mathbf{C}' = \frac{d\mathbf{C}}{dx} = \frac{y'''\left[1+y'^2\right] - 3y'y''^2}{\left[1+y'^2\right]^{(5/2)}} \tag{2}$$

Most parametric splines currently in use (e.g. based on cubic, B-splines, Bezier splines etc) have continuous first and second derivatives and they result in smooth-looking surfaces with continuous curvatures, but discontinuous slopes of curvature at the spline knots. One must distinguish here between: surface roughness and fouling (with which turbomachine blades must operate); and the slope-of-curvature discontinuities in the as-designed shape at the junctions of the splines (which are invisible to the eye, as the blade looks very smooth, but they may produce unusually-loaded blades, higher losses and thicker wakes). The geometry of some blades presented in the literature exhibit slope of curvature disturbances at spline knots along the main part of the blades, affecting boundary layer development, the point of transition etc. Even more blades present a slope of curvature discontinuity where the LE circle or other shape joins the main part of the blade, causing in many cases LE separation bubbles and flow disturbances, which also affect aerodynamic performance. These LE disturbances have recently been systematically studied in compressor leading edges [26, 27]. Overall, this local slope of curvature disturbance or discontinuity has resulted in test and production airfoils (isolated and in turbomachines) that exhibit spikes or dips of various magnitudes in isentropic surface Mach number and pressure-coefficient distribution, which occasionally result in unexpected loading distributions along the blade length and in local separation bubbles. These effects are visible as small local "kinks" in surface pressure or isentropic Mach number distributions in some of the computational and experimental data published, for example, in [28–31], and with local separation bubbles in [32–35].

Blending a leading-edge circle or ellipse with the blade surfaces frequently results in local curvature or slope-of-curvature discontinuities (that may cause local separation bubbles detected only if the test transducers are located at the correct location), or tripping the boundary layer to transition, perhaps with follow-on re-laminarization and re-transition further downstream (with the resultant effects on aerodynamic and heat transfer performance). Such a local leading-edge laminar-separation bubble due to blending of a leading-edge circle with the blade surfaces occurs in the turbine geometry published in [33], seen in the test data published in figure 11 of [35]. This leading-edge separation region was removed by modifying the geometry of the blade in the vicinity of the slope-of-curvature discontinuity with an inverse design technique as explained in figures 11, 12 and 13 of [6]. This is a particularly challenging leading edge separation bubble. Previous attempts with parametric direct blade-design methods to remove this leading edge separation bubble have indicated difficulties [36]; however, later in this paper in an example of the CIRCLE method we show that it can produce a slightly modified blade geometry that removes this separation bubble.

2D TURBINE BLADE DESIGN

Fig. 1 illustrates a typical 2D turbine blade shape, the key LE and TE modifications to the original 2D blade-design method, and the extension of the method to 3D. The inlet and outlet flow angles $\alpha_{in} = \alpha_1$ and $\alpha_{ot} = \alpha_2$, and the throat Mach number M_2 are 3D inputs provided (in the absolute frame for stators and in the relative frame for rotors) from the throughflow calculation. The designer has many additional 3D choices, five of which are crucial: the nondimensional tangential spacing S/b between the

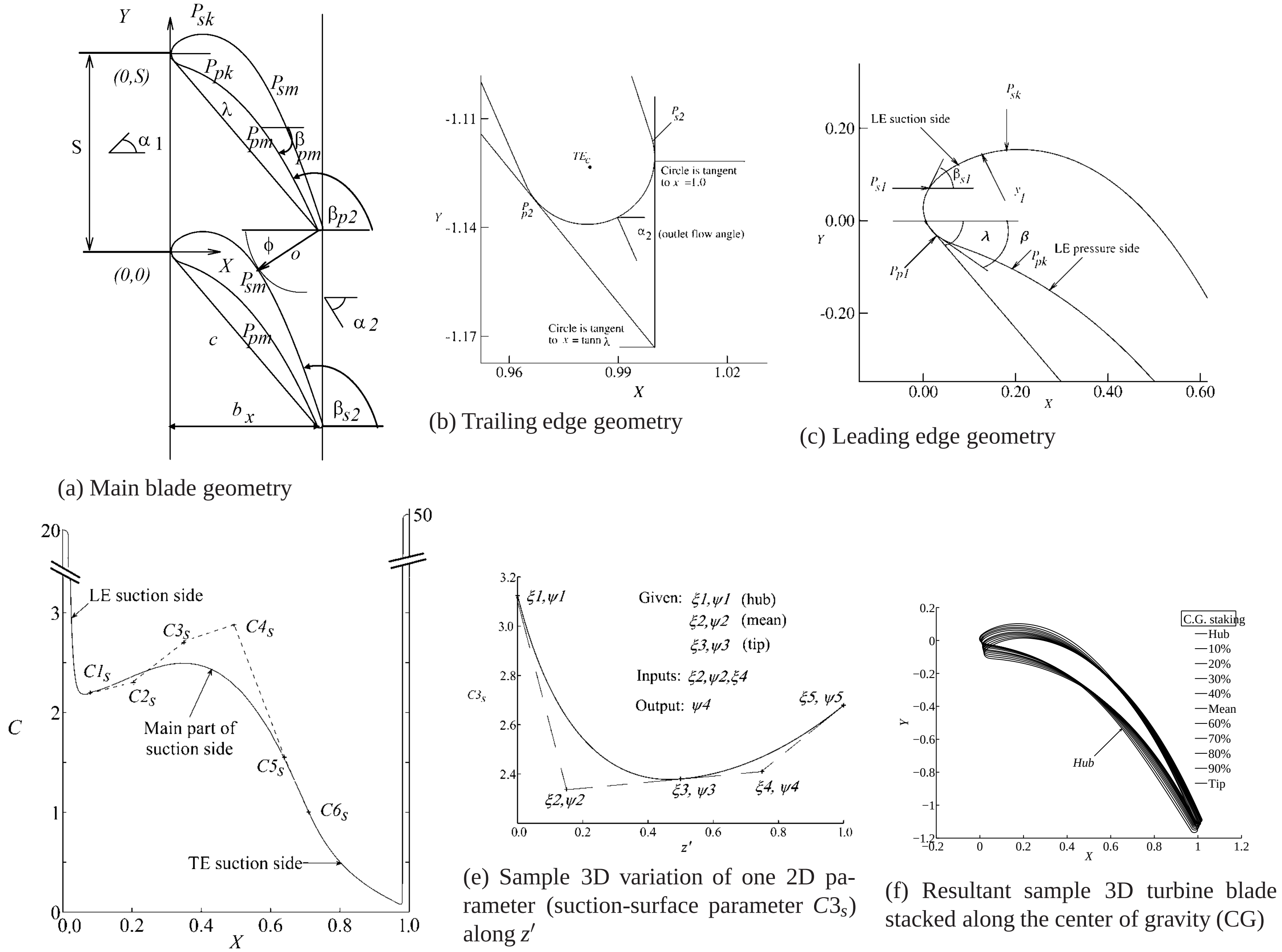

(a) Main blade geometry

(b) Trailing edge geometry

(c) Leading edge geometry

(d) 2D prescribed curvature distribution from leading edge (LE) to trailing edge (TE)

(e) Sample 3D variation of one 2D parameter (suction-surface parameter $C3_s$) along z'

(f) Resultant sample 3D turbine blade stacked along the center of gravity (CG)

FIGURE 1. 2D and 3D blade geometry definition (adapted from [22, 24])

blades (set by the number of blades in the 3D bladerow); the stagger angle λ; the nondimensional throat diameter o/b; and the LE and TE shapes, which without loss of generality can be circles, ellipses, or any other curvature-continuous shape near the stagnation points. These 3D blade-design parameters are functions of blade length from hub to tip, along the blade height (z, z'). The tangential lift coefficient and the drag coefficient are defined by:

$$C_L \equiv \frac{\text{tangential aerodynamic force}}{\text{tangential blade area} \times \text{outlet dynamic head}} \quad (3)$$

$$C_D \equiv \frac{\text{Drag force}}{\text{tangential blade area} \times \text{outlet dynamic head}} \quad (4)$$

These expressions can be manipulated in a number of ways (for compressible flow, for incompressible flow, accounting for variations in axial-flow velocity etc.). The incompressible-flow derivation for turbines [37] reduces C_L to:

$$C_L = 2\frac{S}{b}cos^2\alpha_{ot}(tan\alpha_{in} - tan\alpha_{ot}) \quad (5)$$

The number of blades in the 3D blade row must be chosen so that (approximately) $0.8 < C_L < 1.3$ (the upper value is gradually increasing) in every 2D section from hub to tip. The throat diameter is an extremely important design input because it dictates the mass flow that can be passed through the blade, and hence the work that can be delivered by the turbine. A good *first approximation* is $[o/S] = cos\,\alpha_{ot}$ (from trigonometry in the throat to TE flow region). Experimental data linking o, S, M_2, and the curvature of the convex (suction) blade surface near the trailing edge have been published in the open literature (for instance some are included in [37], where the empirical correlations for α_{ot} are functions of $cos^{-1}[o/S]$). Computer programs can calculate the outlet flow angle for the given blade geometry (i.e. o, S, and M_2).

There is considerable ongoing discussion over LE and TE shapes. For manufacturing reasons the LE and TE of the 3D blade must be made by stacking "consistent" 2D shapes, so circles and ellipses have traditionally been used. Blending these shapes with the blade surfaces introduces slope-of-curvature continuity difficulties such as those illustrated at the leading edge of the Hodson–Dominy (designated HD) blade [6, 33–35], mentioned below in Fig. 4. The trailing-edge thickness should be as small as manufacturing and strength considerations would allow (to minimize the wake incident on the next blade row), and it is affected by geometric constraints imposed by the cooling slots in cooled blades. For compressor and non-cooled blades the trailing edge shape must be joined as smoothly as possible to the blade surfaces. The blade-design method presented in this paper illustrates the use of LE and TE circles. These are the hardest shapes to join to the blade surfaces as there is a transition from the constant curvature of the circle region to the locally varying curvature of the remaining blade surface. Therefore the method presents the most difficult case of joining the LE and TE shapes to the rest of the blade surfaces, and all other shapes will be an easier variation of the methodology presented. Details of the 2D method for pointed TE are in [22, 23]. Details of the 2D LE and TE circles, and 3D concepts are in [24]. A summary of the CIRCLE method is included below in order to facilitate discussion of the results.

The trailing-edge region, $y3$, and TE circle

Each 2D blade section is designed nondimensionally, so that $0 \leq X \equiv x/b \leq 1$ including the leading and trailing edge shapes (Fig. 1a,b,c). Choosing the value of λ and the trailing edge radius locates the trailing edge circle (Fig. 1b). The suction and pressure blade surfaces "detach" from the trailing edge circle at points P_{s2} and P_{p2} specified by input parameters β_{s2} and β_{p2} respectively (local blade-surface angles, determined by the "wedge" blade angle of the trailing edge, and related to the outlet flow angle α_{ot}). The trailing edge region (line segment $y3$) from P_{s2} to P_{sm} on the suction surface is specified by an analytic polynomial $y = f(x)$ of the form:

$$
\begin{aligned}
y3 = f(x) = {} & c_0 + c_1 x + c_2 x^2 + c_3 x^3 + \\
& + c_4 k_1 [x - x(P_{s2})] + c_5 k_2 [x - x(P_{s2})])
\end{aligned} \tag{6}
$$

where k_1 and k_2 are exponential functions resulting in terms of increasing importance as we approach point P_{s2}, and of negligible importance away from P_{s2}. Thus equation 6 is a cubic equation near point P_{sm} where the blade is tangential to the "throat" circle o; and the basic cubic equation has exponential modifications as it approaches the TE circle at point P_{s2}. The six coefficients c_0 to c_5 are evaluated from the conditions of point, first, second and third derivative continuity (four conditions) of the blade surface line at P_{s2}; and prescribing the point and slope of the blade surface line at the tangent to the throat diameter at point P_{sm} (two additional conditions). This approach enables slope of curvature continuity in the vicinity of the trailing edge circle (though the changes in curvature in this vicinity are usually large). The trailing edge region of the pressure surface is specified by a similar polynomial describing a line passing through P_{p2} and P_{pm}, except the blade angle β_{pm} is an input that is not related to the throat circle; it is only related to the location of P_{pm} on the blade surface.

The middle part of the blades, $y2$, and CIRCLE method

The design of the main part of the blades (line segment $y2$) between points P_{sm} and P_{sk} is accomplished by "mapping" the curvature distribution for the shape of the blade surface in that region from the **C** vs. X plane to the Y vs. X plane (fig. 1d). The curvature from P_{sm} to P_{sk} is specified using 4-point to 6-point Bezier splines in curvature, in a manner that ensures curvature *and* slope of curvature continuity from point P_{s2} *through* point P_{sm} to point P_{sk}. For illustration purposes fig. 1d shows a 6-point Bezier spline, though in principle any n-point Bezier spline can be used, and usually 4 Bezier control points are sufficient. The curvature segment corresponding from P_{s2} to P_{sm} is evaluated from analytic polynomial $y3$ of the trailing edge region (using eqn. 6) and plotted on the **C** vs. X plane starting from the TE at $X = 1.0$ and ending in point $C6s$ in fig. 1d. The slope of the curvature $\mathbf{C}_s(x)$ at point $C6_s$ (corresponding to blade point P_{sm}) is computed from eqn. 6 and becomes an input to further calculations. On the curvature of the suction surface we specify points $C1_s$, to $C5_s$. The x location of point $C5_s$ is an input variable, but the value of curvature there is evaluated such that line $C5_sC6_s$ is tangent to the surface-curvature line at point $C6_s$. Point $C2_s$ is user specified. Point $C1_s$ is specified at an x location corresponding to P_{sk}. Since the slope of the Bezier curve is tangent to the line of knots at its ends, the tangency condition at point $C6_s$ ensures slope-of-curvature continuity from $C1_s$ to $C6_s$ (from P_{sk} to P_{s2}). Using central differences equation 1 is written as:

$$
\mathbf{C}_i = \frac{CF1/CF2}{CF3} \tag{7}
$$

$$
CF1 = 2\left(\frac{y_{i+1} - y_i}{x_{i+1} - x_i} - \frac{y_i - y_{i-1}}{x_i - x_{i-1}}\right)
$$

$$
CF2 = (x_{i+1} - x_{i-1})
$$

$$CF3 = \left\{ \left[\frac{1}{2} \left(\frac{y_{i+1} - y_i}{x_{i+1} - x_i} + \frac{y_i - y_{i-1}}{x_i - x_{i-1}} \right) \right]^2 + 1 \right\}^{3/2}$$

From the above equation given (x_{i-1}, y_{i-1}), (x_i, y_i), x_{i+1} and $\mathbf{C}_i$ we can compute y_{i+1}. This can be done by manipulating equation 7 into a sixth-order linear algebraic equation in y_{i+1}, or by a numerical (e.g. regula-falsi) solution. This is solved starting from blade points P_{sm} and progressing explicitly blade point by blade point towards the leading edge to points P_{sk}. The Bezier spline is iteratively manipulated until the slope and the y location of the blade surface at points P_{sk}, and the shape of the curvature distribution, is acceptable. The development of the pressure surface geometry from P_{pm} to P_{pk} is similar using pressure-side control points $C1_p$ to $C6_p$ on $\mathbf{C}_p(x)$.

Leading-edge geometry, $y1$, and the LE circle

The leading edge has dominant effects on aerodynamic and heat transfer performance. Both direct and inverse design methods indicate designing this region requires particular care (e.g. [11,25–27,38]). In this area we implement a hybrid method based on modifications of the earlier methods [20, 22, 24] and illustrated in fig. 1c. First we introduce the LE shape, such as a circle or ellipse, but any other shape that can be manufactured can also be used. Given the foremost point of the blade will be on the y axis ($x = 0$), the stagger angle λ and the radius of the LE circle specify the location of the LE circle as shown in fig. 1c. The suction and pressure blade surfaces "detach" from the LE circle at points P_{s1} and P_{p1} specified by input parameters β_{s1} and β_{p1} respectively (local blade-surface angles, determining the "wedge" blade angle at the LE, and related to inlet flow angle $\alpha_{in} = \alpha_1$). Then a parabolic construction line is defined, and a thickness distribution is added perpendicularly to the construction line (as in [19,20,22]). The construction line starts from a key geometric point such as the origin, the LE of the blade, and in some cases it can start from the center of the LE circle. The thickness distribution of eq. 9 is added perpendicularly about this parabolic construction line, and it is evaluated so that the thickness distribution (and therefore also the blade surface) has continuous point, first, second and third derivative (continuous y, y', y'', y''' and therefore continuous $\mathbf{C}'$) at points P_{s1} (where it joins the LE circle) and P_{sk} (where it joins line segment $y2$ and the main part of the blade).

The suction-side construction line passing though the center of the leading edge circle is (for instance) of the form:

$$y(x) = Ax^2 + Bx + C \tag{8}$$

and the thickness distribution y_t added perpendicularly to the construction line (in order to subsequently arrive at the coordinates of the leading edge segment $y1$) is of the form

$$\begin{aligned} y_t = \quad & c_0 + c_1 x + c_2 x^2 + c_3 x^3 + \\ & + c_4 k_{11} (x - x(P_{s1})) + c_5 k_{12} (x - x(P_{sk})) + \\ & + c_6 k_{13} (x - x(P_{s1})) + c_7 k_{14} (x - x(P_{sk})) \end{aligned} \tag{9}$$

where functions k_{11}, k_{12}, k_{13} and k_{14} are exponential polynomials which acquire increasing importance as we approach points P_{s1} and P_{sk} on the blade surface, so that eqn. 9 is a cubic polynomial away from these two end points. The eight parameters of the thickness function c_0 to c_7 are derived from the conditions to match: y, y', y'' and y''' (and thus $\mathbf{C}'$) at point P_{s1}; and at point P_{sk} respectively. This approach ensures continuity of curvature and slope of curvature from the TE circle to the main part of the blade surface through the leading-edge thickness distribution and into the LE circle. The procedure is similar for the pressure side of the blade.

3D TURBINE BLADE DESIGN

Fig. 1e illustrates the extension of the 2D blade design method to 3D by showing, as one example, the variation of input parameter $C3_s$ (one of the 2D CIRCLE method Bezier control points in fig. 1d) with a Bezier curve in 3D, i.e. its variation along the fraction of blade length z' measured from hub to tip. (Many parameters are a function of blade height z from the throughflow calculation, and they are transferred to z'). Flow angles $\alpha_{in}(z)$ and $\alpha_{ot}(z)$ are outputs of the throughflow calculation and become inputs to the 3D blade design. The hub and tip diameter and the number of blades dictate the blade pitch in each 2D section $S(z)$. Additional inputs specified by the user are $o(z)$, $\lambda(z)$, and $b(z)$. For instance $o(z)$ and $\lambda(z)$ can be specified at the hub, mean and tip radii, and these key values can be used to provide smoothly varying distributions of o and λ along z and z' using Bezier curves as described for $C3_s$ below. Similarly $b(z)$ may be constant from hub to tip, or it may vary along z, thus providing an additional input to control $C_L(z)$ in each 2D section (eqn. 5). These parameters can be constant from hub to tip, or smoothly varying functions of z. Finally, the centers of gravity of the 2D sections can be stacked in any radial orientation, such as along the radius, to reduce the bending moment experienced by the spinning blades; or axial sweep, or lean (dihedral, leaning of the blade perpendicular to the stagger angle or in the tangential direction) may be introduced in the 3D shape. For subsonic designs the values of α_{in} and α_{ot} usually vary smoothly along z from hub to tip, and the resulting radial variations in these blade-design input parameters are also smooth and relatively easy to specify. In each 2D section the shapes of $\mathbf{C}_s$ and $\mathbf{C}_p$ specifying the 2D blade sections (fig. 1d) can be used to manipulate the streamwise curvature distribution of the blade. Local variations in curvature can be used to front, mid or aft load the pressure distribution in each 2D blade section as described in [22, 23]. Increasing the value of λ in each 2D section results in thinner and more front-loaded blades [22].

Typically we obtain the mean blade design (at $z' = 0.5$) as a 2D section, and with either big or small changes in the blade parameters (α_{in}, α_{ot}, λ etc) along the blade height we also obtain the near-hub (at $z' \approx 0.0$) and near-tip (at $z' \approx 1.0$) 2D blade geometries. Each of these three "dominant" 2D blade sections is manipulated until it has the desirable 2D aerodynamic performance at design and off-design incidence, in the manner described in the previous section. This gives values for each one of the 2D blade design parameters at $z' = 0.0, 0, 5, 1.0$. Next, we prescribe the 3D variation of each 2D blade design parameter with Bezier curves in the radial direction in the manner illustrated in fig. 1e. For instance for the blade design parameter denoting the value of point $C3_s$ (fig. 1d), we have input values: $(\xi 1, \psi 1)$ at $z' = 0.0$; $(\xi 3, \psi 3)$ at $z' = 0.5$; and $(\xi 5, \psi 5)$ at $z' = 1.0$. We provide as additional inputs for the radial variation of $C3_s$ Bezier-curve control points $(\xi 2, \psi 2)$ and $\xi 4$. Then the Bezier curve shown in fig. 1e gives as an output the missing value of the control point, $\psi 4$. By specification the resultant Bezier curve in fig. 1e provides a smoothly varying description of $C3_s$ from hub to tip of the blade. The Bezier curve specifying the 3D variation of any blade design parameter may be: convex; concave; or nearly "linear".

The 3D CIRCLE method can provide sharper local variations of 3D parameters than those shown in fig. 1e for transonic and supersonic bladerows. The method can be extended to radial and mixed-flow turbomachines by a coordinate transformation ((x, y) along the streamlines and z perpendicular to streamlines.)

INTEGRATION WITH OPTIMIZATION METHODS

The exact location of the n points controlling 2D curvature such as C1, C2, ... to C6 (fig. 1d) in each 2D section is not as critical as the resulting shape of the curvature distribution; but these input parameters are also specified as smoothly varying along z with the Bezier curves in figure 1e. The resultant shapes can be stacked, for instance along the center of gravity of the sections, resulting in 3D blade shapes like the one illustrated in fig. 1f. Desired changes in 3D surface pressure or 3D streamlines are compared with changes in 3D curvature distributions and the location of the 3D blade surfaces. After the first iteration (first geometric design and analysis) the user examines the resulting 3D blade loading distributions and decides where to increase and decrease local curvature (and local loading). After the second iteration the user gains an appreciation of the magnitude of the required changes in curvature to cause the desired 3D changes in Mach number or pressure distribution, or other aspects, such as the passage vortex and flows near endwall regions. The procedure is repeated until a desirable 3D blade geometry and aerodynamic performance are obtained.

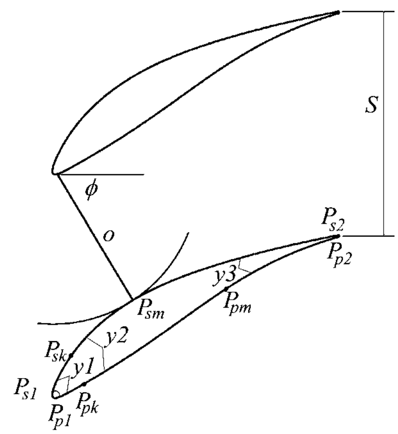

FIGURE 2. Modification for the 2D compressor blade design method

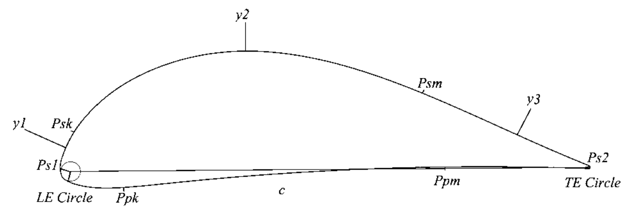

FIGURE 3. Modification for the 2D isolated airfoil blade design method

Each run of the 2D blade-performance Reynolds-averaged Navier-Stokes (RANS) computation with FLUENT shown in this paper take 2-4 hours on a high performance personal computer. The corresponding Euler calculations like the ones in [22] for similar blade geometries take about 1 minute each. The design of a new 2D blade section would start with about 20 Euler calculations followed by about 5 RANS calculations. The above procedure can be automated with used-defined optimization functions, and simple or complex, visual or codified multi-objective heuristic or evolutionary-algorithm optimization methods, e.g. [13–18].

EXTENSION TO 2D and 3D COMPRESSOR BLADES

The 2D compressor blades are specified in a similar manner to 2D turbine blades, as illustrated in fig. 2. One difference is that the "throat" of the 2D section o occurs near the inlet of the bladerow. Again, the blade is defined by LE and TE circles or ellipses connected with line segments $y1$, $y2$ and $y3$ separated by points P_{s2}, P_{sm}, P_{sk}, P_{s1} similarly to the 2D turbine-blade CIRCLE method, and the blade surface curvature and slope of curvature are (by specification) smooth and continuous from the TE stagnation point through points P_{s2}, P_{sm}, P_{sk}, P_{s1} to the LE stagnation point. The 3D compressor blade design parameters are specified by Bezier curves as in fig. 1d.

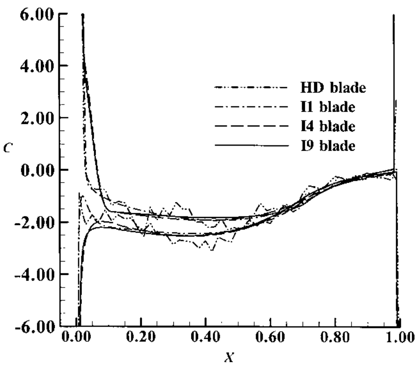

(a) surface curvatures

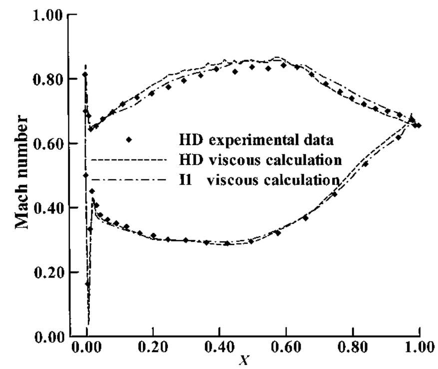

(b) HD experiments with RANS HD and I1 computations

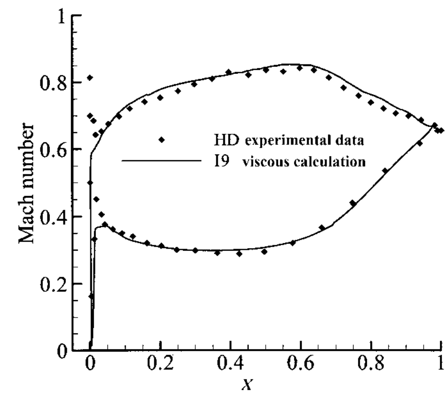

(c) HD experiments with RANS I9 computations

FIGURE 4. Comparison of original HD blade (from [33–35]) with redesigned I1 and I9 blades (adapted from [25])

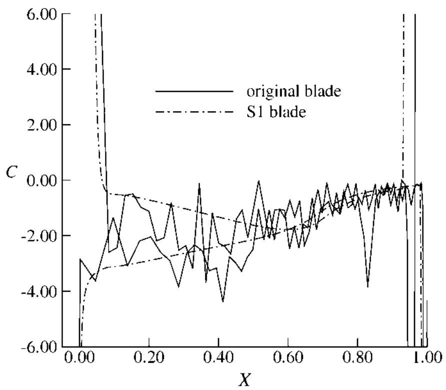

(a) Surface curvatures

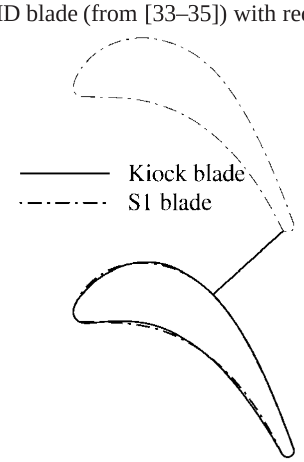

(b) Blade geometries

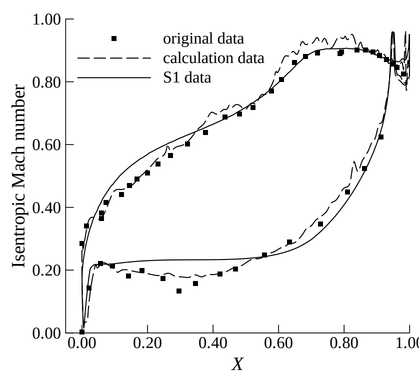

(c) Isentropic surface Mach numbers

FIGURE 5. Comparison of original Kiock blade (from [39]) with redesigned S1 blade

EXTENSION TO 2D and 3D ISOLATED AIRFOILS

The 2D isolated airfoils are specified in a similar manner to 2D turbine and compressor blades, as illustrated in fig. 3. One difference is that there is no “throat”. In this case points P_{sm} and P_{pm}, and blade angles at these locations β_{sm} and β_{pm} are user specified. This gives the opportunity to specify these points at the maximum airfoil thickness thus relating this design aspect to the usual “maximum thickness” and “location of maximum thickness” specifications of the usual isolated airfoil design methods. Again the blade is defined by LE and TE circles or ellipses connected with line segments $y1, y2$ and $y3$ separated by points $P_{s2}, P_{sm}, P_{sk}, P_{s1}$ similarly to the 2D turbine- and compressor-blade CIRCLE methods, and the airfoil surface curvature and slope of curvature are by specification smooth and continuous from the TE stagnation point through points $P_{s2}, P_{sm}, P_{sk}, P_{s1}$ to the LE stagnation point. The 3D airfoil design parameters are specified by Bezier curves as in fig. 1d.

SAMPLE 2D TURBINE BLADE REDESIGNS

Figure 4 shows aspects of the geometry and aerodynamic performance of blade HD [33–35] and redesigned blades I1, I4 and I9. The HD blade profile is a thin, hollow, castable root section from the rotor of a low-pressure turbine. It was designed to operate at air inlet flow angle 38.8° relative to the axial direction and to provide approximately 93° of flow turning. The test $Rey = 2.3 \times 10^5$. Further experimental details can be found in [33–35]. Joining the leading edge circle with the blade surfaces causes local flow discontinuities and a suction side laminar separation bubble, after which the flow re-attaches and becomes turbulent further downstream.

Figure 4a shows the curvature distribution of the original HD blade (jagged line, evaluated numerically from the original blade data points) and of blades I1, I4 and I9. We have restricted the geometry to use the same leading-edge circle diameter, and in order to maintain the same blade chord from $X = [0, 1]$, as the blade became progressively thinner near the leading edge, we limited the reduction in the leading edge wedge angle so that the foremost point of the four blades is at $X = 0$. The surface curvature distributions of blades I1, I4 and I9 are smoother lines, as these blades have been designed with the CIRCLE method. The figure also shows the curvature of blade I1 trying to follow the curvature of the HD blade in the vicinity of the leading edge with a curvature "spike" on the suction side. This "spike" in the surface curvature of blade I1 (which we would not normally use in this region of a blade design) is now required in order to reproduce the flow spike of the HD blade in blade I1. The "spike" is not "prescribed" in the curvature distributions of blades I4 and I9, which are smooth by specification and design. The resultant computed isentropic Mach number surface distributions are shown in fig. 4b and 4c. The sharp local acceleration-deceleration region on the pressure side of the leading edge of blade I9 has also been smoothed.

Mesh generator GAMBIT and flow solver FLUENT have been used in the RANS computations throughout this paper. The mesh elements used for the HD and I1, I4 and I9 blades are: 19,705 quadrilateral cells; 38,967 2D interior faces; and 20,148 nodes for all zones. A 12-layer structured O-mesh with $y^+ < 5$ was used around the blades, and a pave mesh consisting of structured and unstructured regions was used in the passage. The 4-equation $k-\omega$ SST-transition model has been used for the calculations throughout the results shown in this paper. The separation and re-attachment points have been predicted accurately for the HD blade. The mass-averaged stagnation pressure loss computed for the HD blade is $Z_L = 0.00316$ and for the I9 blade $Z_L = 0.00220$. (The computed pressures were recorded along the inflow and outflow boundaries, then weighted by the local mass-flow rates, and finally integrated and averaged at inlet and at outlet boundaries.)

Figure 5 shows RANS computations and comparison with the experimental results of the turbine blade tested by Kiock et. al. [39], and RANS computations of blade S1, redesigned with the CIRCLE method. The experimental results shown are for M_{in} =0.260, M_{ot} =0.782, α_{in} =30°, and α_{ot} =-67.33°. The same type and detail of grid as for the above HD case has been used in the computations. The experimental and computational data for the original blade show disturbances on the suction surface M_{is} at $X \approx 0.1, \approx 0.5$ and ≈ 0.8, and on the pressure surface an acceleration-deceleration region at $X \approx 0.05$. Fig. 5a shows the surface curvature distributions for the original blade (jagged lines, evaluated numerically from the original data points) and the curvature distributions for the redesigned S1 blade (smooth lines). The surface M_{is} of blade S1 is much smoother, and the acceleration-deceleration region on the pressure surface at $X \approx 0.05$ has been removed. The boundary layer of the redesigned blade is thinner than the original blade throughout the suction surface, and as a result the computed mass-weighted average stagnation pressure loss for the Kiock blade is Z_L =0.0134; and for the S1 blade is Z_L =0.00967.

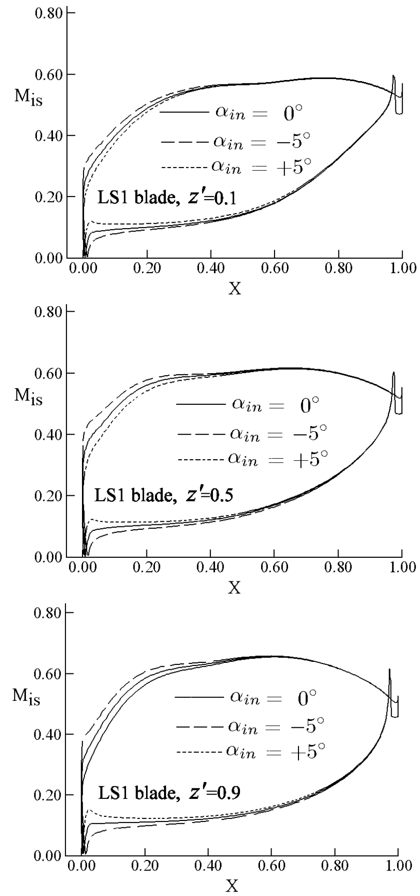

FIGURE 6. Isentropic surface Mach number distributions of the bladerow of fig. 1f at $z' = 0.1, 0.5, 0.9$ at design point $\alpha_{in} = 0°$ and at incidence $\pm 5°$

SAMPLE 3D TURBINE BLADE DESIGN

Figure 6 shows the surface Mach number distributions near the hub ($z' = 0.1$), mean ($z' = 0.5$), and near the tip ($z' = 0.9$) regions of low pressure turbine LS1 designed with inlet total pressure 532 kPa and inlet total temperature 1000 K, inlet flow angle $\alpha_{in} = 0°$, and outlet static pressure 442.7 kPa. The inlet flow angle at design point has been chosen in order to illustrate the capabilities of the blade design method as applicable to isolated airfoils and the removal of leading edge separation bubbles. The Mach number distributions have been computed using GAMBIT and FLUENT in RANS solutions with 10% freestream turbulence and the 4-equation $k-\omega$SST-transition model, with RANS grids similar to those described for the previous blade solutions. The resultant blade geometries can be stacked by the centers of gravity, or the leading edges, or the trailing edges, and they are shown stacked by the centers of gravity in fig. 1f. Additional variations in sweep and dihedral can be used to account for the passage vortex, flows in endwall regions, and other 3D effects.

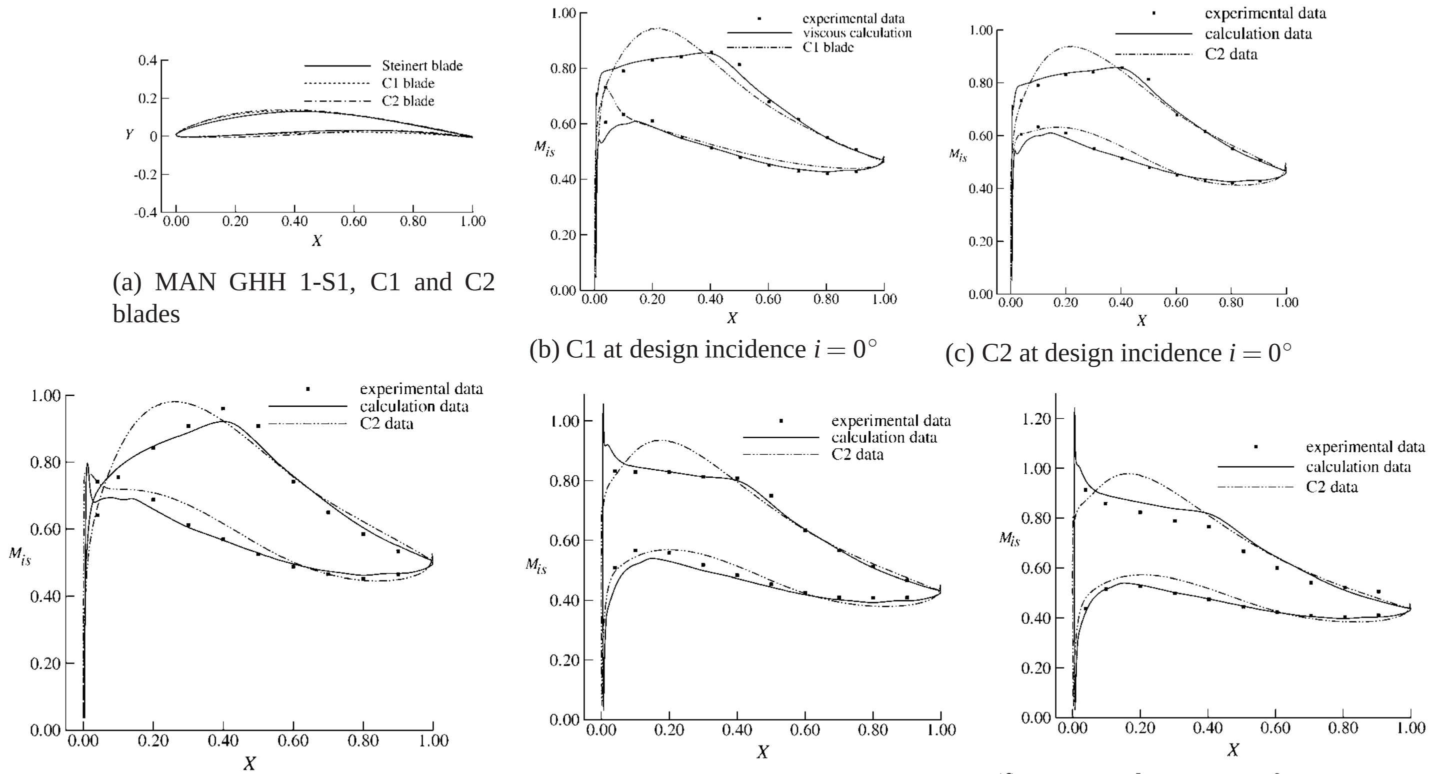

(a) MAN GHH 1-S1, C1 and C2 blades

(b) C1 at design incidence $i = 0^\circ$

(c) C2 at design incidence $i = 0^\circ$

(d) C2 at incidence $i = -4^\circ$

(e) C2 at incidence $i = +4^\circ$

(f) C2 at incidence $i = +5^\circ$

FIGURE 7. Comparison of MAN GHH 1-S1 (Steinert, from [8]) with C1 and C2 compressor blades at various incidences

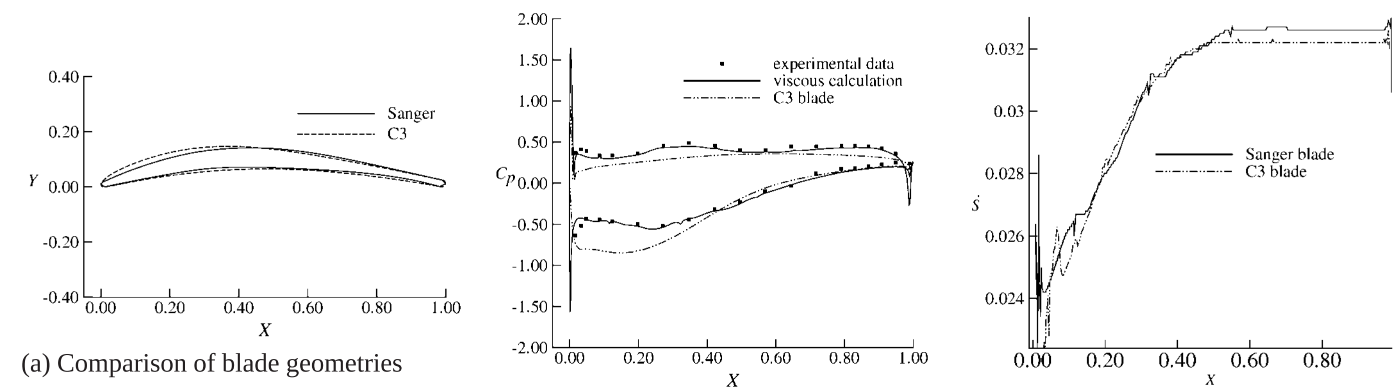

(a) Comparison of blade geometries

(b) Comparison of C_p distributions

(c) Comparison of entropy generation

FIGURE 8. Comparison of Sanger (from [40]) and C3 compressor blades at design point incidence

SAMPLE 2D COMPRESSOR BLADE REDESIGNS

Fig. 7 shows a comparison of the geometry and aerodynamic performance of the high-subsonic Mach number MAN GHH 1-S1 compressor blade with redesigned blades C1 and C2 at design and off-design incidences $\pm 4^\circ$ and +5°. The experimental points are from [8]. The solid lines are RANS computations of the original blade shape, and the dashed lines are the RANS computations of the redesigned C1 and C2 blades. The mesh elements used for the computations are: 30,520 quadrilateral cells; 60,558 2D interior faces; and 31,000 nodes for all zones. A 2D O-mesh and a Pave-unstructured mesh consisting of a combination of structured and unstructured regions have been used. The mesh around the airfoil consisted of twenty one structured clustered O-grid layers with wall boundary parameter $y^+ < 1$. The remaining flow field was discretized with quadrilateral and a small numbers of triangular cells. The 4-equation $k-\omega$ SST-transition model has been used. The experimental conditions for this blade are: $p_{o,in} = 101{,}325$ Pa; inlet stagnation temperature 287.15 K; turbulence intensity 1.5%, turbulence length scale $l_m/chord = 0.0476$; M_{in} =0.618; and pressure ratio 1.1021. Further experimental details can be found in [8]. The original blade exhibits LE "spikes" on the pressure side at negative incidence, and on the suction side at positive incidence. Blade C1 is the first redesign attempt, and it exhibits an acceleration-deceleration regime on the pressure side near the LE. This has been largely removed in the second redesign attempt, in blade C2. The computed boundary layers are thinner, tolerance to incidence is increased, and the rates of entropy generation are lower along the surfaces of blade C2 than the original blade. As a result the losses are lower, as shown in Table 1.

TABLE 1. Computed pressure-loss parameters of the original MAN GHH 1-S1 (Steinert) and C2 compressor blades

Blade	Design and off design incidence, i				
	$-7°$	$-4°$	$0°$	$+4°$	$+5°$
original, Y_L	0.0466	0.0232	0.0186	0.0176	0.0417
C2, Y_L	0.0148	0.0142	0.0158	0.0171	0.0188
C2, Z_L	0.0029	0.0022	0.0017	0.0018	0.0028

Fig. 8 shows a comparison of the Sanger controlled diffusion compressor blade with redesigned blade C3 at design point incidence. The experimental conditions are: $p_{o,in}$ =1.03 atm; M_{in} =0.25; inlet stagnation temperature 294 K; $p_{st,ot}$ =1.00 atm; Rey =7×10^5. Further experimental details are in [40]. The results of RANS computations on the original and CIRCLE-redesigned blade C3, using a grid of similar fidelity to that of the Steinert blade, and the 4-equation $k-\omega$ SST-transition model, are shown in fig. 8. The suction- and pressure-side LE "spikes" of the original blade have been removed. Fig. 8c shows a comparison between the computed rate of entropy creation inside the boundary layer of the suction side of the Sanger and the redesigned C3 blades. As in the other cases, this reduction of boundary layer losses results in a decrease of the mass-averaged stagnation pressure losses.

SAMPLE 2D ISOLATED AIRFOIL REDESIGN

Fig. 9 shows a comparison of the geometry and aerodynamic performance of the original Eppler 387 and of the redesigned A1 airfoils. The $Rey = 10^5$; turbulence intensity is 0.5%; and $i_{crd} = +4°$. Further experimental details can be found in [41].

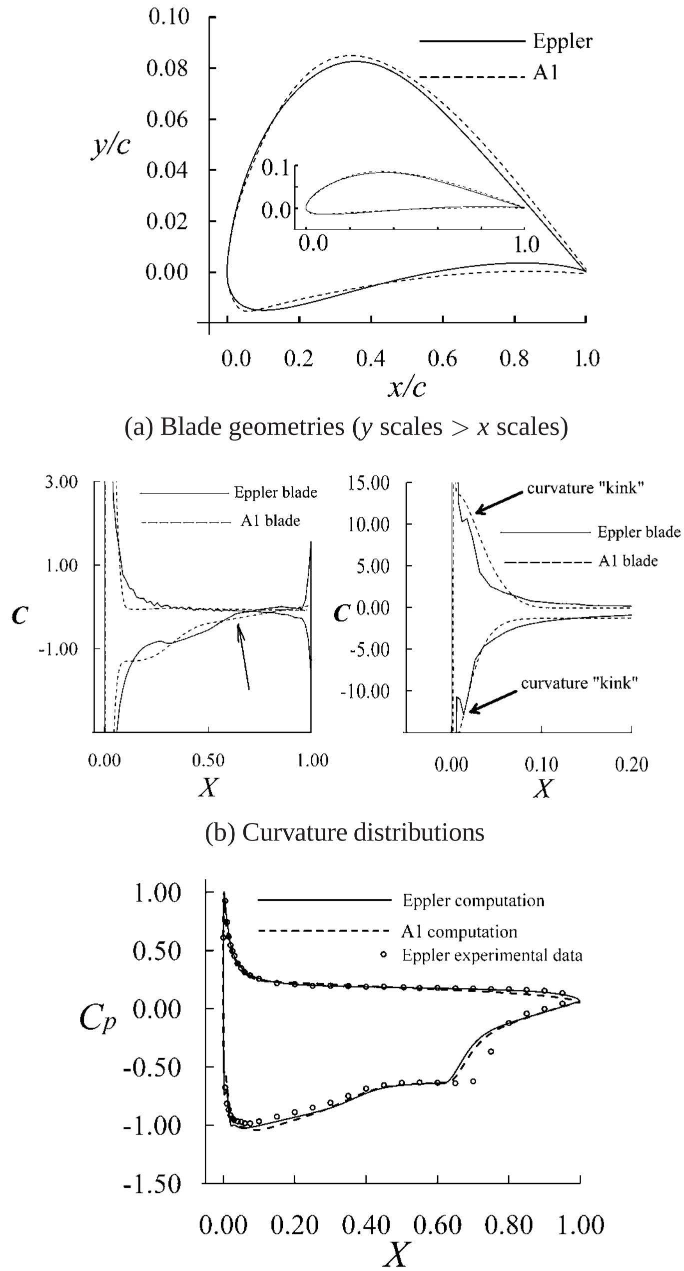

(a) Blade geometries (y scales > x scales)

(b) Curvature distributions

(c) C_p distributions

FIGURE 9. Comparison of Eppler 387 (from [41]) and A1 isolated airfoils

2D structured C (for pointed TE Eppler) and O (for circular TE A1) meshes with 50 y points and clustering around the LE region have been constructed around the airfoils with $y+\leq 1.2$; surrounded by an unstructured Pave C mesh extending 12 chords upstream and 20 chords downstream of the airfoil, with a total number of about 350,000 grid points. The solid line is the RANS computation of the original airfoil shape, and the dashed line is the RANS computation of the redesigned A1 airfoil using the 4-equation $k-\omega$ SST-transition model (fig. 9c).

The computations indicate a small acceleration-deceleration flow-disturbance region near the LE on the suction side of the original airfoil, shown here as a small "kink" in the computed C_p distribution in the calculations for the original airfoil, where

$$C_p \equiv \frac{\text{static pressure on the surface}}{(1/2)\times(\text{upstream fluid density})\times(\text{upstream fluid velocity})^2} \quad (10)$$

This small LE flow disturbance, caused by a small curvature disturbance ("kink") in that region, has been removed with the CIRCLE airfoil design method in the redesigned airfoil A1.

The computations indicate that at this *Rey* the boundary layer on the suction surface of the Eppler airfoil remains laminar until $X \approx 0.6$. After that the momentum of the boundary layer near the surface is insufficient to carry the flow, and there is a laminar separation bubble in that region. The RANS computations on the Eppler airfoil indicate that the flow reattaches turbulent further downstream at $X = 0.677$. The original Eppler airfoil has a small slope-of-curvature discontinuity on the suction surface at $X \approx 0.6$. Despite the removal of this slope of curvature discontinuity in airfoil A1 (fig. 9b), the laminar separation at $X \approx 0.6$ is a characteristic of the Reynolds number of the flow and the local diffusion required by both airfoils.

As a result of the removal of the curvature "kink" near $X = 0.01$ and the slope of curvature discontinuity near $X = 0.6$ the laminar separated region starts a little later in airfoil A2 than in the Eppler airfoil; and the flow also reattaches turbulent a little later in the A2 airfoil, at $X = 0.680$. There is a reduction in losses between the original Eppler 387 and redesigned A1 airfoil as a result of the overall improvement of the curvature of the airfoil surface, reflected in: a drop in C_D from 0.0207 to 0.0181; and a corresponding rise of C_L/C_D from 38.68 to 41.94. Additional wind-turbine airfoil examples have been presented in [42].

CONCLUSIONS

The CIRCLE method to design 2D and 3D subsonic, transonic or supersonic blades for axial compressors and turbines, and isolated blades or airfoils is presented. The method, which can be easily coupled to multi-objective heuristic or evolutionary-algorithm optimization methods, is based on prescribing the streamwise 2D suction- and pressure-surface curvatures from leading to trailing edge of the blades. This curvature and slope of curvature continuity includes the locations where the suction and pressure surfaces join the leading and trailing edge circles, ellipses, or other shapes, so that curvature and slope of curvature are smooth and continuous everywhere along the blade surfaces from LE stagnation point to TE stagnation point.

In the 3D method the 2D sections of the hub, mean and tip (or near hub and tip) are designed first. Then the 2D blade surface curvature distributions in the hub, mean and tip sections is manipulated until a desirable aerodynamic performance at design point flow as well as at incidence flow is obtained, avoiding local flow acceleration-deceleration regions and other flow disturbances in these three sections. Then the 2D blade-design parameters are smoothly varied from hub to tip with Bezier curves in the radial direction, providing a smooth variation of 2D blade sections from hub to tip. The 3D variation of these blade design parameters is iteratively manipulated until a desirable aerodynamic performance from hub to tip is obtained. The 2D blade sections are stacked from hub to tip along the centers of gravity, or the leading, or the trailing edge, or with another stacking strategy. The method can be further enhanced using the results of 3D flow computations to direct the 3D variation of the blade design parameters. The resultant 3D blades exhibit superior aerodynamic characteristics, while concurrently the designer has full control of blade structural characteristics. The use of the 3D method is illustrated with a turbine bladerow example.

Variations of the 2D and 3D method for turbine blades, compressor blades and isolated airfoils are presented.

This is a new design environment decoupling the traditional maximum thickness and maximum camber discussions (used in early airfoil designs) from blade design, and it attaches greater significance to the curvature distribution rather than the exact location of (x,y) points on the blade, even though the designer has direct control of the blade surface as in direct methods. Similarly to inverse design methods, the CIRCLE method is guided by the surface pressure and surface Mach number distributions with their relation to surface-curvature distribution, and the output is the blade shape. The design sequence shapes the surface curvature and with it the location of maximum loading, forwards or backwards, on the blade surface. Therefore this method combines the best advantages of direct and inverse blade design methods.

Different methods to control the differences in the surface curvature, especially between the LE shape and the rest of the blade, have been proposed, for instance [43–47]. The computed results indicate that the CIRCLE method is the most successful blade-design method in the open literature in controlling this "LE spike" difficulty between the LE shape and the rest of the blade. The method also ensures smooth surface pressure distribution throughout the blade surfaces, and allows for smooth changes in blade geometry and loading distribution, while ensuring high-efficiency blades are designed.

The aerodynamic advantages of the CIRCLE blade design method in designing improved blades (of lower losses) are illustrated with two examples of 2D axial turbines, two examples of 2D axial compressors, one 2D isolated airfoil, starting from blade geometries with tested experimental performance, and designing new blades with improved computed performance and of increased tolerance to incidence. It is concluded that the method is a new design environment enabling design of higher-efficiency turbomachine blades.

ACKNOWLEDGMENT

The authors acknowledge the contributions of MSc and PhD students, and postdocs, who over two decades have contributed to coding various aspects of the CIRCLE blade design method in FORTRAN, C++ and MATLAB, and on various platforms and operating systems: George Pantazopoulos; Nick Vlachopoulos; Paschalis Papagiannidis; Dequan Zou; Richard Binzley; Sean Spicer; Brandon Wegge; Yan Tan; Mingyu Shi; and Akbar Rahideh. The PhD research of Idres Hamakhan was sponsored by the Ministry of Education of Kurdistan; and the PhD research of M. Amin Rezaienia is currently sponsored by Queen Mary, University of London.

REFERENCES

[1] Massardo, A. F., and Scialò, M., 2000. "Thermoeconomic analysis of gas turbine based cycles". *Transactions of the ASME, Journal of Engineering for Gas Turbines and Power*, ***122***, pp. 664–671.

[2] Massardo, A., and Satta, A., 1990. "Axial-flow compressor design optimization. 1. Pitchline analysis and multivariable objective function influence". *Transactions of the ASME, Journal of Turbomachinery*, ***112***(3), July, pp. 399–404.

[3] Massardo, A., Satta, A., and Marini, M., 1990. "Axial-flow compressor design optimization. 2. Throughflow analysis". *Transactions of the ASME, Journal of Turbomachinery*, ***112***(3), July, pp. 405–410.

[4] Pachidis, V., Pilidis, P., Talhouarn, F., Kalfas, A., and Templalexis, I., 2006. "A fully integrated approach to component zooming using computational fluid dynamics". *Transactions of the ASME, Journal of Engineering for Gas Turbines and Power*, ***128***(3), July, pp. 579–584.

[5] Meauze, G., 1989. "Overview on blading design methods". In *Blading design for axial turbomachines, AGARD Lecture Series 167, AGARD-LS-167*. AGARD, May.

[6] Stow, P., 1989. "Blading design for multi-stage hp compressors". In *Blading design for axial turbomachines, AGARD Lecture Series 167, AGARD-LS-167*. AGARD, May.

[7] Bry, P. F., 1989. "Blading design for cooled high-pressure turbines". In *Blading design for axial turbomachines, AGARD Lecture Series 167, AGARD-LS-167*. AGARD, May.

[8] Steinert, W., Eisenberg, B., and Starken, H., 1991. "Design and testing of a controlled diffusion airfoil cascade for industrial axial flow compressor application". *Transaction of the ASME, Journal of Turbomachinery*, ***113***, pp. 583–590.

[9] Selig, M. S., 1994. "Multipoint inverse design of an infinite cascade of airfoils". *AIAA Journal*, ***32***(4), Apr, pp. 774–782.

[10] Dang, T., Damle, S., and Qiu, X., 2000. "Euler-based inverse method for turbomachine blades, Part 2: Three-dimensional flows". *AIAA Journal*, ***38***(11), Nov, pp. 2007–2013.

[11] Phillipsen, B., 2005. A simple inverse cascade design method. ASME paper 2005-GT-68575.

[12] Liu, G.-L., 2000. "A new generation of inverse shape design problem in aerodynamics and aero-thermoelasticity: concepts, theory and methods". *An International Journal of Aircraft Engineering and Aerospace Technology*, ***72***(4), April, pp. 334–344.

[13] Kim, H., Koc, S., and Nakahashi, K., 2005. "Surface modification method for aerodynamic design optimization". *AIAA Journal*, ***43***(4), Apr, pp. 727–740.

[14] Samad, A., and Kim, K. Y., 2008. "Stacking and thickness optimization of a compressor blade using weighted average surrogate model". In Proceedings of the ASME TURBO EXPO 2008, VOL 6, PT A, pp. 2183–2195. 53rd ASME Turbo Expo 2008, Berlin, Gernamy, Jun 09-13, 2008.

[15] Samad, A., and Kim, K. Y., 2008. "Shape optimization of an axial compressor blade by multi-objective genetic algorithm". *Proceedings of the Institution of Mechanical Engineers part A-Journal of Power and Energy*, ***222***(A6), Sep, pp. 599–611.

[16] Kim, J. H., Choi, J. H., and Kim, K. Y., 2009. "Design optimization of a centrifugal compressor impeller using radial basis neural network method". In Proceedings of the ASME TURBO EXPO 2009, VOL 7, PTS A AND B, pp. 443–451. 54th ASME Turbo Expo 2009, Orlando, FL, Jun 08-12, 2009.

[17] Kim, J. H., Choi, J. H., Husain, A., and Kim, K. Y., 2010. "Performance enhancement of axial fan blade through multi-objective optimization techniques". *Journal of Mechanical Science and Technology*, ***24***(10), OCT, pp. 2059–2066.

[18] Kim, J. H., Ahn, H. J., and Kim, K. Y., 2010. "High-efficiency design of a mixed-flow pump". *Science China-Technological Sciences*, ***53***(1), JAN, pp. 24–27.

[19] Korakianitis, T., 1987. "A design method for the prediction of unsteady forces on subsonic, axial gas-turbine blades". Doctoral dissertation (Sc.D., MIT Ph.D.) in Mechanical Engineering, Massachusetts Institute of Technology, Cambridge, MA, USA, September.

[20] Korakianitis, T., 1989. "Design of airfoils and cascades of airfoils". *AIAA Journal*, ***Vol.27***(4), April, pp. 455–461.

[21] Korakianitis, T., 1993. "Hierarchical development of three direct-design methods for two-dimensional axial-turbomachinery cascades". *Journal of Turbomachinery, Transactions of the ASME*, ***115***(2), April, pp. 314–324.

[22] Korakianitis, T., 1993. "Prescribed-curvature distribution

airfoils for the preliminary geometric design of axial turbomachinery cascades". *Journal of Turbomachinery, Transactions of the ASME*, ***115***(2), April, pp. 325–333.

[23] Korakianitis, T., and Papagiannidis, P., 1993. "Surface-curvature-distribution effects on turbine-cascade performance". *Journal of Turbomachinery, Transactions of the ASME*, ***115***(2), April, pp. 334–341.

[24] Korakianitis, T., and Wegge, B. H., 2002. Three dimensional direct turbine blade design method. AIAA paper 2002-3347. AIAA 32nd fluid dynamics conference and exhibit, St. Louis, Missouri, June.

[25] Hamakhan, I. A., and Korakianitis, T., 2010. "Aerodynamic performance effects of leading edge geometry in gas turbine blades". *Applied Energy*, ***87***(5), May, pp. 1591–1601.

[26] Wheeler, A. P. S., Sofia, A., and Miller, R. J., 2009. "The effect of leading-edge geometry on wake interactions in compressors". *Transaction of the ASME, Journal of Turbomachinery*, ***131***(4), pp. 041013–1 – 041013–8.

[27] Goodhand, M. N., and Miller, R. J., 2011. "Compressor leading edge spikes: a new performance criterion". *Transactions of the ASME, Journal of Turbomachinery*, ***133***(2), April, pp. 021006–1 021006–8.

[28] Okapuu, U., 1974. Some results from tests on a high work axial gas generator turbine. ASME paper 74-GT-81, March.

[29] Gostelow, J. P., 1976. A new approach to the experimental study of turbomachinery flow phenomena. ASME paper 76-GT-47.

[30] Wagner, J. H., Dring, R. P., and Joslyn, H. D., 1984. Inlet boundary layer effects in an axial compressor rotor: part 1 - blade-to-blade effects. ASME paper 84-GT-84.

[31] Sharma, O. P., Pickett, G. F., and Ni, R. H., 1990. Assessment of unsteady flows in turbines. ASME paper 90-GT-150.

[32] Hourmouziadis, J., Buckl, F., and Bergmann, P., 1987. The development of the profile boundary layer in a turbine environment. Transactions of the ASME, Journal of Turbomachinery, Volume 109, No. 2, pp. 286-295, April. ASME paper 86-GT-244, 1986.

[33] Hodson, H. P., and Dominy, R. G., 1987. "Three-dimensional flow in a low pressure turbine cascade at its design condition". *Transactions of the ASME, Journal of Turbomachinery*, ***109***(2), Apr, pp. 177–185. ASME paper 86-GT-106.

[34] Hodson, H. P., and Dominy, R. G., 1987. "The off-design performance of a low-pressure turbine cascade". *Transactions of the ASME, Journal of Turbomachinery*, ***109***(2), Apr, pp. 201–209. ASME paper 86-GT-188.

[35] Hodson, H. P., 1985. "Boundary-layer transition and separation near the leading edge of a high-speed turbine blade". *Transactions of the ASME, Journal of Engineering for Gas Turbines and Power*, ***107***, pp. 127–134. ASME paper 84-GT-179.

[36] Corral, R., and Pastor, G., 2004. "Parametric design of turbomachinery airfoils using highly differentiable splines". *Journal of Propulsion and Power, Vol. 20, No. 2, pp. 335-343*, March-April.

[37] Wilson, D. G., and Korakianitis, T., 1998. *The design of high-efficiency turbomachinery and gas turbines*, 2nd ed. Prentice Hall.

[38] Walraevens, R. E., and Cumpsty, N. A., 1995. "Leading edge separation bubbles on turbomachine blades". *Transactions of the ASME, Journal of Turbomachinery*, ***117***, January, pp. 115–125.

[39] Kiock, R., Lehthaus, F., Baines, N. C., and H., S. C., 1986. "The transonic flow through a turbine cascade as measured in four European wind tunnels". *Transaction of the ASME, Journal of Engineering for Gas Turbines and Power*, ***108***(2), April, pp. 277–284. (ASME paper 85-IGT-44, 1985.).

[40] Elazar, Y., and Shreeve, R. P., 1990. "Viscous flow in a controlled diffusion compressor cascade with increasing incidence". *Transactions of the ASME, Journal of Turbomachinery*, ***112***, April, pp. 256–265.

[41] McGhee, R. J., and Walker, B. S., 1988. Experimental results for the Eppler 387 airfoil at low Renolds numbers in the Langley Low Pressure Turbine Tunnel. NASA-TM-4062.

[42] Korakianitis, T., Rezaienia, M. A., Hamakhan, I. A., Avital, E., and Williams, J. J. R., 2011. Aerodynamic improvements of wind-turbine airfoil geometries with the prescribed surface curvature distribution blade design (CIRCLE) method. ASME paper GT2011-46722.

[43] Buche, D., Guidati, G., and Stoll, P., 2003. Automated design optimization of compressor blades for stationary, large-scale turbomachinery. Proceedings of IGTI03 ASME Turbo Expo 2003: Power for Land, Sea and Air, Atlanta, Georgia, USA, June 13-16.

[44] Sieverding, F., Ribi, B., Casey, M., and Meyer, M., 2004. "Design of industrial axial compressor blade sections for optimal range and performance". *Transaction of the ASME, Journal of Turbomachinery*, ***126***(2), pp. 323–331.

[45] Li, H.-D., He, L., Li, Y. S., , and Wells, R., 2006. Blading aerodynamics design optimization with mechanical and aeromechanical constraints. Proceedings of ASME Turbo Expo, GT2006-90503: Power for Land, Sea and Air, Barcelona, Spain, May 8-11.

[46] Lee, K. S., Kim, K. Y., and Samad, A., 2008. "Design optimization of low-speed axial flow fan blade with three-dimensional RANS analysis". *Journal of Mechanical Science and Technology*, ***22***, pp. 1864–1869.

[47] Chen, B., and Yuan, X., 2008. "Advanced aerodynamic optimization system for turbomachinery". *Transactions of the ASME, Journal of Turbomachinery*, ***130***, April, pp. 021005–0210017.